

Indirect Evidence for Lévy Walks in Squeeze Film Damping

S. Schlamminger, C. A. Hagedorn, J. H. Gundlach
*Center for Experimental Nuclear and Particle Astrophysics,
University of Washington, Seattle, WA 98195 USA*

Molecular flow gas damping of mechanical motion in confined geometries, and its associated noise, is important in a variety of fields, including precision measurement, gravitational wave detection, and MEMS devices. We used two torsion balance instruments to measure the strength and distance-dependence of ‘squeeze film’ damping. Measured quality factors derived from free decay of oscillation are consistent with gas particle superdiffusion in Lévy walks and inconsistent with those expected from traditional Gaussian random walk particle motion. The distance-dependence of squeeze film damping observed in our experiments is in agreement with a parameter-free Monte Carlo simulation. The squeeze film damping of the motion of a plate suspended a distance d away from a parallel surface scales with a fractional power between d^{-1} and d^{-2} .

PACS numbers: 05.40.-a, 07.10.Pz, 95.55.Ym, 07.30.-t

The damping of mechanical motion by residual gas particles in vacuum has been the subject of measurement, discussion, and controversy [1–5]. ‘Squeeze film damping’ is enhanced gas damping that occurs due to molecular flow in constrained geometries [6–9]. Quantitative understanding of this damping is essential to a wide range of subjects: The quality factor of many MEMS oscillators is limited by squeeze film effects. In future gravitational wave interferometers, test masses will be suspended within millimeters of another surface, constraining gas flow. The fluctuation-dissipation theorem dictates that squeeze film damping generates noise that may limit these experiments [10].

Noteworthy are two recent publications on squeeze film damping: In Ref. [6] the damping of three topologically different MEMS oscillators suspended a fixed distance from a substrate was measured as function of residual gas pressure. Ref. [7] also measured the damping as function of gas pressure, using two torsion balances centered in closely-spaced housings. Both groups measured greater damping than expected from free gas damping, and developed Monte Carlo simulations that agreed with their experimental data. Ref. [7] drew attention to the importance of constrained gas damping to gravitational wave detectors. As their geometry models the planned LISA gravitational wave detector, which is sensitive to both transverse and longitudinal gas flow, they did not replicate the planar geometry of existing and planned ground-based interferometers. These experiments and the failure of analytic theory to match their results motivated our measurement of the distance dependence of squeeze film damping with a simple planar geometry.

We used two different torsion balances to investigate mechanical damping in rarefied gas. We provide experimental data characterizing the distance and pressure dependence of squeeze film damping using the simple and well controlled geometries of two adjacent surfaces. We compare our data to analytic theory and to Monte Carlo simulations. The simulations indicate that Gaussian random walks incorrectly describe the diffusion of gas particles in narrow gaps. Instead, squeeze film damping,

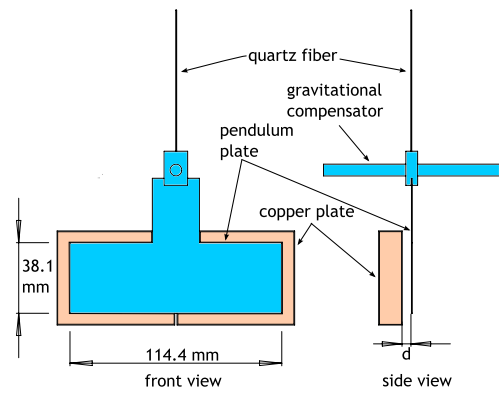


Figure 1. Schematic drawing of the LTA torsion pendulum. The copper plate is mounted on a translation stage allowing gaps up to 9 mm. The pendulum is suspended by a quartz fiber with $Q > 50000$.

including distance-dependence, is better described by superdiffusive particle transport in Lévy walks.

Each of our two torsion balance instruments consists primarily of a thin vertical plate pendulum suspended from a torsion fiber. Each pendulum is parallel to a stationary surface situated a distance d away. We determined the damping by measuring the mechanical quality factor, Q , of each pendulum’s free oscillation as a function of d and as a function of the residual gas pressure P .

The LISA Test Apparatus (LTA) torsion balance [11] depicted in Fig. 1 was constructed specifically to investigate noise sources in LISA. The plate of the LTA torsion pendulum is a 0.45 mm thick Si wafer, 114.4 mm wide and 38.1 mm tall. The plate has a small riser section connecting it to a perpendicular Al bar designed to minimize its sensitivity to fluctuating gravitational fields caused by nearby human activity. The pendulum assembly is suspended from a quartz fiber with intrinsic $Q > 50000$. The assembly has a free period of 120.89 s and a moment of inertia of $9.7 \times 10^{-6} \text{ kg m}^2$. The pendulum plate is positioned parallel to a thick Cu plate. The Cu plate is

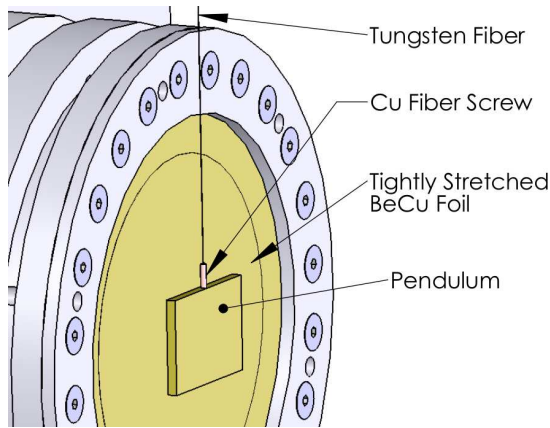


Figure 2. Schematic drawing of the NTA torsion pendulum. The pendulum is suspended by a tungsten fiber with intrinsic $Q \sim 4000$. The pendulum can be translated to change the gap between pendulum and foil.

divided into two halves; both are electrically grounded. The pendulum to Cu-plate gap, d , can be varied between 0 and 9 mm. The Cu plate and pendulum are sputter-coated with Au to reduce contact potentials and patch effects [12]. The total electrical charge on the pendulum was reduced below 0.5 pC [13]; our results were not affected by deliberate increases in charge. The torsion balance is housed within a stainless-steel vacuum chamber. The vacuum is maintained by a small turbo-molecular pump with an extra molecular drag stage backed by a small diaphragm pump.

Our second instrument, the ‘Newton Test Apparatus’ (NTA), is depicted in Fig. 2. A 2.00 mm thick, 42.18 mm wide, and 30.81 mm tall metal plate is suspended from a tungsten fiber near a tightly-stretched 12 μm thick flat beryllium-copper foil. The foil-pendulum gap, d , is varied by moving the torsion fiber suspension point. The pendulum has a free period of 85 s and a moment of inertia of $3.1 \times 10^{-6} \text{ kg m}^2$. Like in the LTA, both foil and pendulum are coated with Au. The torsion balance is housed within a stainless-steel vacuum bell jar and the vacuum is maintained by a turbo-molecular pump.

The torsional motion of each pendulum is monitored with a laser autocollimator.

To determine the size of the gap and to assure proper alignment between the pendulum plates and their adjacent surfaces in LTA and NTA, several methods were employed: (1) Calibrated photographs were taken through vacuum windows. (2) Each pendulum was allowed to twist in both directions until the pendulum’s outer edge touched the adjacent surface. The gap was determined by the maximum twist angles and the size of the pendulum plate. (3) In the LTA, the capacitance between the two halves of the copper plate was measured as a function of d and was fit to a capacitance model. Discrepancies between the distance measurements determined the uncertainty $\sigma_d = 0.1 \text{ mm}$ in LTA, 15 μm in NTA. The parallelism, about the horizontal axis, of the pendulums

w.r.t the adjacent surfaces was better than 0.5 mrad in LTA and 30 μrad in NTA. The parallelism about the vertical axis was better than 0.15 mrad in LTA and 0.6 mrad in NTA. Systematic and flatness distance uncertainties were $< 45 \mu\text{m}$ in LTA and $< 23 \mu\text{m}$ in NTA.

To improve confidence in our pressure measurement, we connected five ion gauges from three different manufacturers and a variable leak valve to a single small vacuum chamber. With the exception of one suspect gauge, the gauges agreed to within 30% over the range of 10^{-4} – $2.6 \times 10^{-2} \text{ Pa}$. From this set, a cold-cathode gauge was used for all of the LTA measurements and a hot cathode gauge was used for all of the NTA measurements. We calibrated the hot-cathode ion gauge with a simple pressure-division apparatus. With it, we verified the gauge linearity and calibrated the gauge absolutely to within $2 \times 10^{-3} \text{ Pa}$. Our experiments were carried out at a temperature of $297 \pm 1 \text{ K}$.

In the LTA, the pressure was adjusted by changing the speed of the turbo pump and allowing the apparatus to come into equilibrium. Data were taken at three different pressures. The pressure at the gauge was $\sim 10\%$ smaller than the pressure in the chamber due to gas pumping impedances. We measured the composition of the gas in the chamber with a residual gas analyzer at all three working pressures. H_2O (18 amu) and N_2 (28 amu) together accounted for at least 85% of the residual gas. At the working pressures of 2×10^{-3} , 1×10^{-4} , and $4 \times 10^{-5} \text{ Pa}$, the partial pressure ratios ($p_{18}:p_{28}$) were 0.4:1, 2:1, and 8:1, respectively. Nitrogen is pumped more efficiently at high turbo pump speeds.

In the NTA, measurements were made by pumping the vacuum vessel below 10^{-4} Pa , closing the turbo pump’s roughing valve, and turning the turbo pump off. Q measurements began after the turbo had stopped ($P \geq 9 \times 10^{-4} \text{ Pa}$). The pressure in the chamber rose at a constant rate, most likely due to outgassing from the chamber walls. Data were taken with pressure rises of 1.3 – $7 \times 10^{-7} \text{ Pa/s}$ until the pressure reached 1.3 – $2 \times 10^{-2} \text{ Pa}$. We assume that the residual gas was primarily particles with mass 18 amu, as we expect the outgassing to be dominated by water.

We measured the free decay of each pendulum’s torsional mode to determine Q . The LTA torsion pendulum was excited to an oscillation amplitude of 0.9 mrad. The pendulum motion was recorded for $> 10000 \text{ s}$. The data were cut into segments two oscillation periods in length. The data in each cut were fit to $\theta(t) = A \cos(2\pi ft) + B \sin(2\pi ft) + C$. The extracted amplitudes were then fit to an exponential decay to extract Q , where the amplitude $\theta(t) = \theta_0 e^{-\pi ft/Q} = \sqrt{A(t)^2 + B(t)^2}$. Errors of 20% were deemed to be conservative overestimates in all cases. In the NTA, data recordings of $> 1000 \text{ s}$, with initial amplitude 0.2–4 mrad, were fit to $\theta(t) = e^{-\pi t/TQ} (A \cos(2\pi t/T) + B \sin(2\pi t/T)) + C + Dt$, where A, B, C, D, T , and Q were fit simultaneously. This procedure allowed measurements while the gas pressure was slowly varied. Seismic noise and other excitations

conservatively limit our ability to measure Q to < 50000 in the LTA and < 1500 in the NTA.

The inverse of the measured quality factors, as functions of pressure and pendulum-plate separation, are presented in Figs. 4 and 5.

In the molecular flow regime, where the particle mean free path is much larger than the gap and particle interactions may be neglected, gas damping is primarily due to ‘unconstrained gas damping’ and ‘squeeze film damping’. All of our data were taken in this regime.

In unconstrained gas damping, the motion of an object is retarded by collisions with ambient gas particles. A rectangular plate of dimensions $a \times b$ moving perpendicular to its surface with velocity u through a dilute gas is retarded by the force: $F(u) = -\alpha Pab\langle v \rangle^{-1}u$, with $\langle v \rangle = \sqrt{8k_B T/(\pi m)}$, m the gas particle mass, the ambient pressure P and temperature T . Three values for α can be found in the literature: $\alpha = 16/\pi$ [4, 9], $\alpha = 16$ [2], and $\alpha = 24$ [1]. Unconstrained gas damping depends linearly on the gas pressure but is independent of the gap to nearby surfaces.

Squeeze film damping of two adjacent plates moving towards each other arises because the gas between the plates is temporarily compressed until the “trapped” gas can diffuse out of the gap and restore equilibrium with the surrounding gas. To compute the dissipative force on the plate we start with Suijlen’s derivation [6]. Periodic motion of the plate with amplitude $z_0 \ll d$ and angular frequency $\omega \ll \langle v \rangle/d$ will cause the distance-dependent squeeze film force on the moving plate:

$$F = -\frac{abP}{d} \frac{(\omega\tau)^2 + i\omega\tau}{1 + \omega^2\tau^2} z_0, \quad (1)$$

where the diffusion time, τ , for particles to enter or leave the gap is discussed in detail below.

For a torsional oscillator, the damping forces must be converted to torques. We approximate the torsion pendulum as two $a \times b$ plates with lever arm $a/2$. We expect that a more precise model would give only small corrections to this approximation. For a torsion balance with resonant frequency $f_0 \ll 1/\tau$ and moment of inertia I , we find that the inverse of the quality factor Q is:

$$\frac{1}{Q} = \frac{a^3 b P}{4\pi I f_0 \langle v \rangle} \left(\alpha + \frac{\langle v \rangle \tau}{d} \right). \quad (2)$$

Since Suijlen *et al.* [6] and Cavalleri *et al.* [7] found that their experimental results and simulation disagreed with Gaussian theoretical expectations, we undertook our own simulation effort to determine the diffusion time τ . We simulated gas particles traveling interaction-free in the gap. Initially, particles were randomly distributed throughout the gap volume and assigned three-dimensional velocities according to the Maxwell-Boltzmann distribution. Upon collision with a wall, the particles were emitted with a polar angular distribution

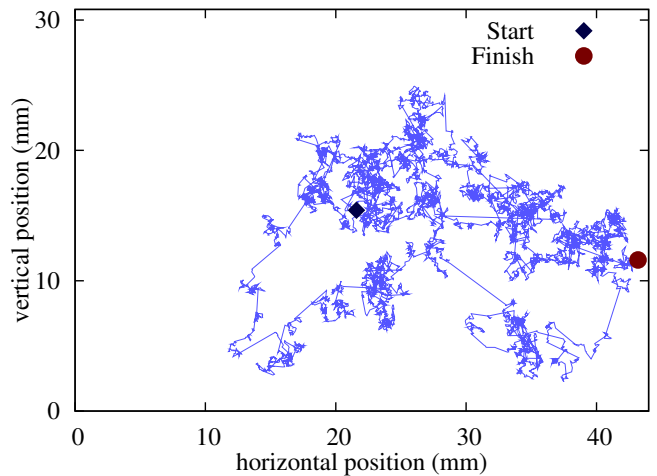


Figure 3. Simulated trajectory of a gas particle in the NTA experiment for a 0.1 mm gap. The occasional large steps are a consequence of the infinite variance of the step-size distribution. These steps, which lead to superdiffusion, and scale-invariance are characteristic of Lévy walks.

$p(\theta)$ and a Maxwellian velocity distribution. The angular and velocity distributions of desorbed particles are poorly understood. A review, [14], suggests that $p(\theta) \propto \cos^n \theta$ with $n \geq 1$, where the traditional choice, $n = 1$, is motivated by time-reversal symmetry. The particles were tracked until they left the volume, and the time at which they left the gap was recorded. The average of these times, for 10000 trials, was taken as the simulated diffusion time. For the setup for which Suijlen *et al.* provide a complete description of their geometry, our results agree.

Simulated particle tracks (Fig. 3) show occasional very long steps. These long steps are essential for understanding squeeze film damping.

Assuming thermal equilibrium and $p(\theta) \propto \cos \theta$, the probability for a particle to make a step of length r_s with a duration t_s is given by

$$p_1(r_s, t_s) dr_s dt_s = \frac{64d^2 r_s \exp(-\frac{4(d^2 + r_s^2)}{\pi t_s^2 \langle v \rangle^2})}{\pi^2 t_s^4 \langle v \rangle^3 (d^2 + r_s^2)^{1/2}} dr_s dt_s. \quad (3)$$

The length of the step, r_s , is measured parallel to the plates. r_s and t_s are not independent, but the distribution of each can be obtained by integrating $p_1(r_s, t_s)$ over the other. For example, the steps are distributed as $p_1(r_s) dr = 2d^2 r_s / (d^2 + r_s^2)^2 dr_s$, consistent with [6]. The step-size and time-of-flight distributions have infinite variance, indicative of Lévy flights/walks. In a Lévy flight the time to make a step is independent of step length. In a Lévy walk the particle travels with finite velocity [15–18], as in a physical gas. The defining feature of Lévy flights/walks is that repeated application of the step-size distribution leads to a stable, scale-invariant distribution with infinite variance. The Lorentzian is an example of such a distribution. Our Monte Carlo simulations show that $p_N(r)$ becomes scale invariant after a few bounces. Lévy walks can lead to superdiffusive

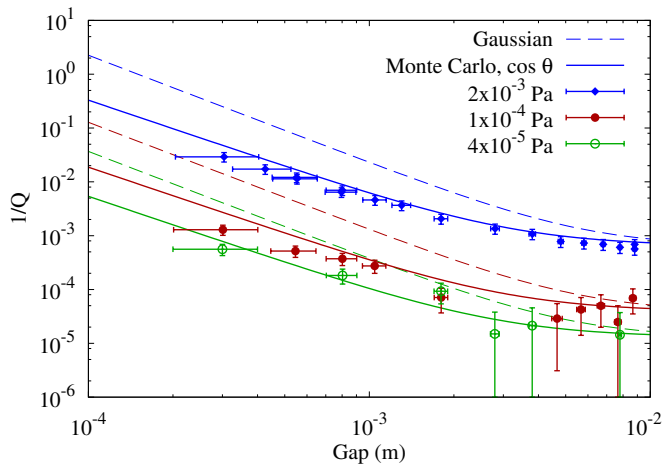


Figure 4. The dissipation factor ($1/Q$) as a function of plate-pendulum separation at constant pressure in the LTA. The lines are calculated using Eq. 2 with the diffusion time τ determined by the parameter-free Monte Carlo simulation (solid) and the Gaussian diffusion equation (dashed). The curves flatten with increasing gap as unconstrained gas damping begins to dominate. The residual gas composition changes with pressure; the curves are calculated using the five measured leading gas species at each pressure.

behavior [15, 18], i.e. the mean square displacement of an ensemble of particles released at $r = 0$ increases as $\langle r_N^2 \rangle \propto t^\gamma$, with $\gamma > 1$. Our Monte Carlo simulation of gas particle trajectories trapped between two infinite planes shows $\gamma \approx 1.15$, independent of d , for $t \gg d/\langle v \rangle$, i.e. after a few bounces. $\langle r_N^2 \rangle$, in contrast to $\langle r_s^2 \rangle$, remains finite because $\langle r_N^2 \rangle$ is evaluated using the position of all particles in free flight between collisions with the two planes.

The smooth curves in figures 4 and 5 are computed using Eq. 2, with $\alpha = 16$. The dashed lines are calculated with the Gaussian diffusion time, $\tau = 8ab/(\pi^3 d \langle v \rangle)$ [6], and the solid lines are computed using our Monte Carlo diffusion times. The dotted line in Fig. 5 is computed using the same simulation but with an angular distribution of emitted particles $p(\theta) \propto \cos^2 \theta$. As the damping is expected to be linear in pressure, we also plot $1/(QP)$ for the NTA. We cannot do so for the LTA results, as the residual gas species change with pressure. The lines in Fig. 4 are calculated with the measured residual gas composition.

Our squeeze film measurements are inconsistent with Gaussian diffusion. In Eq. 2, for small d , Q is proportional to d^β , where β depends on the diffusion time, $\tau(d)$. For $\tau \propto d^{-1}$ (Gaussian diffusion), $\beta = 2$ and for constant τ , $\beta = 1$. We find $\beta = 1.4 \pm 0.3$ in LTA and 1.6 ± 0.3 in NTA. Our Monte Carlo simulations predict $\beta = 1.73$ in LTA and 1.85 in NTA. The data are consistent with our simulations using $p(\theta) \propto \cos^n \theta$ for $n = 1$ and clearly inconsistent for $n \geq 2$. The measured Q is inversely proportional to gas pressure, as predicted in Eq. 2.

We have made the first rigorous measurement of the

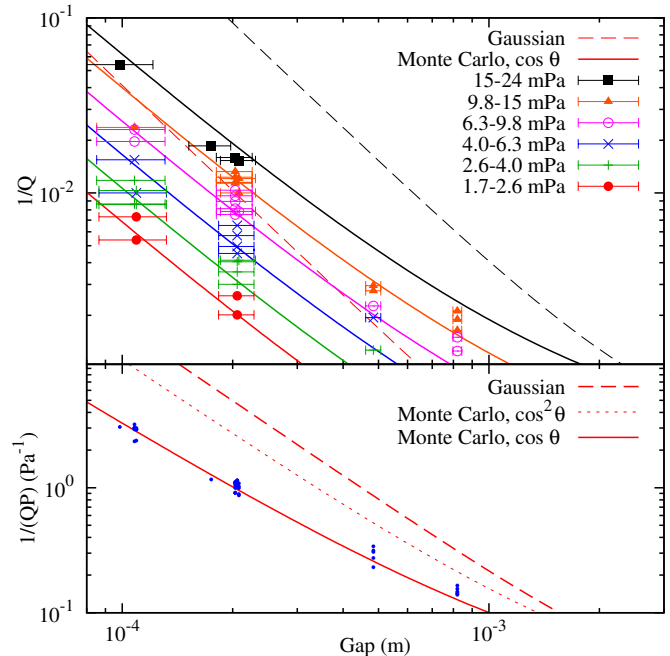


Figure 5. Dissipation factor as a function of pendulum-foil separation in the NTA. The lines are calculated as in Fig. 4. The lower panel shows the dissipation factor divided by the pressure. These data agree well with our Monte Carlo prediction (solid line), which has superdiffusive Lévy-like behavior. The data are inconsistent with Gaussian theory (dashed line) and with a desorption angular distribution $p(\theta) \propto \cos^n \theta$, for $n \geq 2$ (dotted line).

distance dependence of squeeze film damping by adjusting the gap between an oscillator and a flat plane. Experiments in two separate instruments were performed using planar geometries such that the gas flow is restricted by a single gap. This geometry is analogous to the geometry in existing gravitational wave interferometers and simpler than the geometry of the experiments described in Ref. [7]. We point to the connection between squeeze film damping and the theory of Lévy walks. The infinite variance of the step-size distribution of Lévy walks leads to superdiffusion, which is consistent with our data. These measurements are simple examples of microscopic Lévy phenomena in nature. In addition, our results support a cosine angular distribution of re-emission of adsorbed gas particles. As predicted by our Monte Carlo simulation, the measured squeeze film damping is smaller and less dependent on gap size than expected by Gaussian theory. The comprehensive data set presented here can be used to verify any Monte Carlo simulation of squeeze film damping. Squeeze film damping must be considered as a limitation of next-generation gravitational wave detectors. The design of these detectors requires precise knowledge of the strength and distance dependence of squeeze film damping.

We thank Rainer Weiss for stimulating conversation. This work was supported by NASA grant NNX08AY66G, by NSF grant PHY0653863, and by DOE funding for the

-
- [1] B. Li *et al.*, Sens. Actuators A **77**, 191 (1999).
[2] Z. Kádár *et al.*, Sens. Actuators A **53**, 299 (1996).
[3] J. D. Zook *et al.*, Sens. Actuators A Phys. **35**, 51 (1992).
[4] R. Christian, Vacuum **16**, 175 (1966).
[5] C. A. Hagedorn, S. Schlamminger, and J. H. Gundlach, in *Laser Interferometer Space Antenna: 6th International LTA Symposium*, Edited S.M. Merkowitz and J. Livas, American Institute of Physics Conference Series Vol. 873, pp. 189 (AIP, Melville, New York, 2006).
[6] M.A.G. Suijlen *et al.*, Sens. Actuators A **156**, 171 (2009).
[7] A. Cavalleri *et al.*, Phys. Rev. Lett. **103**, 140601 (2009).
[8] M. Bao and H. Yang, Sens. Actuators A **136**, 3 (2007).
[9] S. Hutcherson and W. Ye, J. Micromech. Microeng. **14**, 1726 (2004).
[10] P.R. Saulson, Phys. Rev. D **42**, 2437 (1990).
[11] S. Schlamminger *et al.*, in *Laser Interferometer Space Antenna: 6th International LTA Symposium*, (ref. [5]), pp 151.
[12] S. E. Pollack, S. Schlamminger, and J. H. Gundlach, Phys. Rev. Lett. **101**, 071101 (2008).
[13] S. E. Pollack *et al.*, Phys. Rev. D **81**, 021101(R) (2010).
[14] G. Comsa and R. David, Surf. Sci. Rep. **5**, 145 (1985).
[15] J. Klafter, M.F. Shlesinger, and G. Zumofen, Phys. Today **49**, 33 (1996).
[16] M.F. Shlesinger, G.M. Zaslavsky, and J. Klafter, Nature **363**, 31 (1993).
[17] M.F. Shlesinger, J. Klafter, and G. Zumofen, Am. J. Phys. **67**, 1253 (1999).
[18] E. Barkai, Chem. Phys. **284**, 13 (2002).